Electronic Supplementary Material (ESI) for Physical Chemistry Chemical Physics.
This journal is © the Owner Societies 2019

Electronic Supplementary Information for the article

Hydrophobic pattern of alkylated ureas markedly affects water rotation and hydrogen bond dynamics in aqueous solution

Bogdan A. Marekha[a] and Johannes Hunger*[a]

Experimental

Samples

All alkyl ureas studied in the present work (nominal purity ≥ 98 %) were purchased from TCI chemicals, Germany, and used without further purification. Solutions were prepared by weight in 4 % D_2O (99.9 % D, Sigma Aldrich) – H_2O (MilliQ) solvent mixtures and sonicated for 30 min. All concentrations are reported in molality scale, ***b*** [m]: moles of solute per kg of solvent. For IR experiments samples were contained between two 2-mm-thick CaF_2 windows separated with a Teflon spacer. The thickness of the spacer varied from 25 to 50 μm so that the maximum absorbance in the 2500 cm^{-1} spectral region ranged from 0.3 to 0.6. All measurements were performed at 22 °C.

Linear FTIR

Linear absorption spectra were recorded in transmission with a 2 cm^{-1} resolution using a Nicolet Magna-IR 850 Series II FTIR spectrometer equipped with a DTGS detector. The spectrum of an empty sample cell was taken as reference.

Femtosecond pump-probe experiments

Infrared pulses centred at ~4 μm (2500 cm^{-1}) were generated from 800 nm pulses (~50 fs, 1 kHz repetition rate) produced by a Ti-sapphire-based regenerative amplifier (Spitfire Ace, Spectra-Physics). The 800 nm light was used to pump an optical parametric amplifier (TOPAS-Prime, Spectra-Physics) to produce signal (~1.3 μm) and idler (~1.9 μm) beams. The signal and idler beams were combined in a non-collinear difference-frequency generation (NDFG) stage based on a GaSe crystal yielding ~200 fs long tunable mid-IR pulses (~15 μJ pulse energy) with ~ 350 cm^{-1} spectral bandwidth (FWHM).

The mid-IR light was split into three beams using a wedged CaF_2 window: the front- and back-reflections (~4 % of the total pulse energy each) were used as reference and probe beams, respectively, while the transmitted beam (~90%) served as pump beam. The latter was sent through a computer-controlled mechanical delay stage to control the waiting time, T_w, and then focused and spatially overlapped in the sample together with the probe beam using a gold-coated off-axis parabolic mirror. The pump beam was dumped after the sample and the probe beam was re-collimated using a parabolic mirror and focused, together with the reference beam, on the entrance slit of a monochromator (Triax 180 from Horiba Scientific). The probe and reference beams were dispersed by the monochromator using 150 grooves/mm grating onto two rows of a liquid nitrogen cooled mercury-cadmium telluride (MCT) array detector (2 × 32 pixels, InfraRed Associates, Inc.), providing a spectral resolution of ~9 cm^{-1} in the studied spectral range. The reference beam intensity was used to correct for probe pulse energy fluctuations on a shot-to-shot basis.

For active noise suppression we modulate the pump beam at 500 Hz. From the measured probe, I^{j}_{probe}, and reference, I^{j}_{ref}, intensities in the presence ($j = on$) and absence ($j = off$) of the pump, we obtain pump-induced time- and frequency-dependent modulation of the probe absorption, $\Delta\alpha(\tilde{\nu}_{probe}, T_w)$:

$$\Delta\alpha(\tilde{\nu}_{\mathrm{probe}}, T_w) = -\ln \frac{I^{on}_{probe}/I^{on}_{ref}}{I^{off}_{probe}/I^{off}_{ref}} \qquad (S1)$$

We rotate the pump polarization by 45 ° with respect to the probe polarization using a half-wave plate. A motorized wire-grid polarizer after the sample allows selecting probe light

components parallel or orthogonal to the pump polarization.[1] From both polarization components we construct the isotropic signal, $\Delta\alpha_{iso}$, which only reflects the population relaxation

$$\Delta\alpha_{iso} = \frac{\Delta\alpha_{\parallel} + 2\Delta\alpha_{\perp}}{3} \qquad (S2)$$

and the anisotropy parameter, R, which is a measure for memory of the excitation polarization

$$R = \frac{\Delta\alpha_{\parallel} - \Delta\alpha_{\perp}}{3\Delta\alpha_{iso}} \qquad (S3)$$

The anisotropies were constructed after subtracting the isotropic contribution of the heated ground state, as obtained from the isotropic model, from the raw data (see below for details of the model).[2]

2D-IR experiments

2D-IR experiments were based on a similar combination of regenerative amplifier and OPA (Coherent Astrella, TOPAS Prime OPA and NDFG), which delivers ~20 µJ IR pulses at 1 kHz repetition rate centred around 2500 cm^{-1} with ~200 fs pulse duration. The IR light was guided to a commercial 2D-IR spectrometer (2D-Quick, PhaseTech Inc.) operating in a pump-probe geometry. A small portion of the IR light is split off using a ZnSe wedge and is divided into probe and reference beams using a beam splitter. The larger fraction of the IR light was sent to a pulse-shaper based on a Ge acousto-optic modulator (AOM).[3,4] The shaped IR pump pulse energy at the sample was around 2 µJ. The third order non-linear signal from the sample heterodyned with the probe pulse was collected in the frequency domain by spectrally dispersing in a spectrograph using a 70 grooves/mm grating on a liquid nitrogen cooled MCT array detector (128 by 128 pixels) providing the $\tilde{\nu}_{probe}$ axis resolution of ~2 cm^{-1} in the studied

wavenumber range. The pump frequency was resolved in the time domain using the pulse shaper to create pump pulse pairs with controlled delays (coherence times) and phases.[3,4] We collected absorptive spectra in the rapid-scan mode[5] using four-frame phase cycling to suppress background scattering and transient absorption contributions. To reduce the number of scanned coherence times we shift the phase using the rotating frame.[3,4] Raw data containing 100 increments of 15 fs step size were apodized with the Hamming window and zero-padded to 256 data points in the time domain before Fourier transformation to the frequency domain.[4] This provided the numerical resolution of ~2 cm^{-1} along the $\tilde{\nu}_{pump}$ axis.

The delay between the probe and the pump pulses (T_w) was controlled *via* a motorized delay stage. The zero delay time was established by following the dynamics of the induced absorption in a thin Ge plate placed at the sample position with the pulse shaper operating in a pump-probe mode.[6,7] The pump-probe signal in Ge was also used to optimize group velocity dispersion (GVD) correction parameters for the pulse shaper.[7] The 2D-IR spectra were recorded with the pump polarization parallel to the probe polarization (<*ZZZZ*> polarization combination).[4]

Isotropic transient absorption data

To study the effect of RUs on inter- and intramolecular coupling of the HOD, we perform infrared pump-probe experiments. In these experiments the spectral changes and dynamics after excitation of the *v*(OD) bands are probed as function of delay time (waiting time, T_w) and probe frequency, $\tilde{\nu}_{probe}$. The isotropic transient absorption data,[1] $\Delta\alpha_{iso}$, are free of

reorientational contributions and only reflect vibrational energy relaxation dynamics. We find these dynamics to be very similar in all the studied alkyl urea solutions.

As illustrated by a sample dataset of 4 *m* 1-EU in Figure S1A, at short waiting times the isotropic transient absorption spectra are dominated by a negative contribution (bleach or increased transmission) around 2500 cm^{-1} originating from a reduced absorption from the vibrational ground state |0> due to its population depletion and from stimulated emission from the first excited state |1>. Adjacent to this bleach, the onset of a positive feature below *ca*. 2420 cm^{-1} due to pump-induced absorption of the excited *v*(OD) population (excited state absorption, ESA), which is red-shifted with respect to the fundamental mode due to anharmonicity,[8] is observed. Within approximately 5-10 ps depending on the solute concentration, the isotropic signal plateaus, and persists up to 100 ps time scales.[8] The long time-delay transient spectrum can be described by a difference spectrum between the thermally equilibrated ('hot') ground state after vibrational energy dissipation and the unperturbed ground state.[9,10] Its spectral shape reflects a slight blue shift of the spectrum of the thermalized ground state with respect to the unperturbed ground state as a result of a net weakening of the hydrogen bonding network as the excess energy is dissipated in low frequency modes.

Relaxation from the initially excited state to the 'hot' ground state involves at least two characteristic times scales (for example see the 2440 cm^{-1} trace in Figure S1B: a fast ~2 ps rise is followed by a slower decay). Qualitatively, the isotropic transient spectra of *v*(OD) in solutions of alkyl ureas are very similar to that reported for HOD in neat H_2O[9] as well as in solutions of both urea[11] and TMU.[12–14] To quantitatively describe the relaxation dynamics, we

employ the same kinetic model that was used in these reports. In this model the excited state population decays exponentially with a time constant τ_1 to an intermediate state |0'>. The latter subsequently decays to the thermalized ground state |0*> with a time constant τ^*. The intermediate state |0'> accounts for a delayed appearance of the heated ground state |0*> as the excitation energy cascades down to the manifold of low frequency modes. The data in the 2400-2650 cm^{-1} wavenumber range can be excellently described by this biexponential cascading model assuming frequency independent dynamics (see solid lines in Figure S1). An example of relative contributions to the isotropic transient absorption data of the different states thus obtained is presented in Figure S1A. As vibrational relaxation proceeds, the contribution of the heated ground state |0*> increases. Relative spectral contribution of the intermediate state |0'> is minor as its population decays rather quickly (~1 ps time scale) to the thermalized end-level.

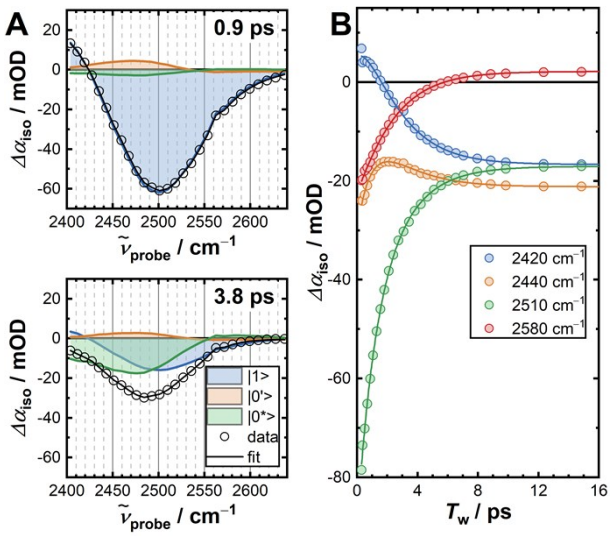

Figure S1. ***(A)*** *Isotropic transient spectra of v(OD) of trace HDO in 4 m 1-EU solution at two selected waiting times together with the fit and the transient spectral contributions due to the populations of the excited state |1>, intermediate level |0'> and the thermalized end-level |0*>.* ***(B)*** *Corresponding isotropic time traces at selected probe wavenumbers.*

The values of τ_1 and τ^* (Figure S2) indicate that all studied RUs moderately slowdown vibrational relaxation dynamics of the solvent to the same extent (*ca.* by 20% at 5 *m*), in line with literature reports for TMU[12]. Conversely, these dynamics were reported to remain unaffected by U up to very high solute concentrations.[11,15] Therefore, regardless of the substitution pattern, RUs truncate the hydrogen bonded network of water such that vibrational energy dissipation dynamics are slowed-down. This implies rather weak sensitivity of the *v*(OD) vibrational relaxation dynamics to the excluded volume of non-hydrogen bonding moieties of an amphiphilic solute.

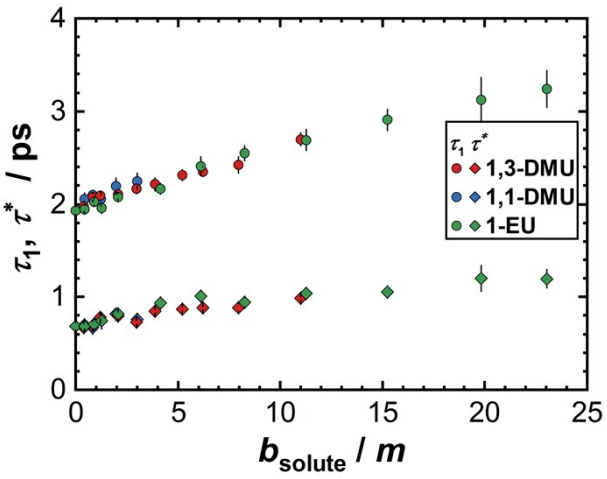

Figure S2. Lifetimes of the vibrationally excited state |1> (τ_1, circles) and of the intermediate state |0> (τ^*, diamonds) of the HOD v(OD) vibration in solutions of the studied alkyl ureas in 4 % D_2O/H_2O as a function of solute molality b_{solute} obtained from the fits of the isotropic data to a model described in the text. The error bars correspond to a 4 % increase of the weighted sum of squared deviations.*

Fitting model of the anisotropic data

The time-dependent anisotropy, $R(T_w)$, obtained from pump-probe data after subtracting the time-dependent contribution of the thermalized ground state (for details see ref 9), was averaged around the bleach central frequency (±10 cm^{-1}). It is described as a mole-fraction-weighted average of contributions from bulk-like water and from non-bulk-like water whose dynamics are slowed down by the solute. The former is modelled by an exponential decay and the latter is represented by a constant offset, which implies much longer rotational time scales, outside the accessible time-window:[11]

$$R(T_w) = R_0\{f_b e^{-T_w/\tau_{bulk}} + f_s\} \qquad (S4)$$

where R_0 is the anisotropy value at zero waiting time, f_s is the fraction of water molecules with slower reorientational dynamics than in bulk-like water, $f_b = 1 - f_s$ is the corresponding bulk-like fraction, τ_{bulk} is the characteristic time scale of bulk-like water reorientation. To avoid potential bias due to temporal overlap of the pump and probe pulses at early times[4] or contributions of faster librational motions,[16] we fit the model only at T_w > 500 fs. For a given RU, we perform a simultaneous weighted fit of eq. S4 to the data at different solute concentrations together with a dataset for the neat solvent. The parameter τ_{bulk} is assumed to be independent of RU concentrations and the value of f_s is fixed at zero for the neat solvent dataset. The thus obtained values for τ_{bulk} (2.5±0.2 ps) agree well with reported values for HOD in H_2O.[9,16]

The proposed above model (eq. S4) implies that the 'slow' water fraction is essentially immobile at the time scale of the observed anisotropy decay. Given that molecular dynamics

simulations suggest a rather moderate retardation,[17] we also analyze our data, using a different estimate for the rotation time of the slowed-down water molecules, τ_{slow}: We estimate τ_{slow} from a typical relaxation time of the 'slow' water mode (25 ps) observed in the dielectric spectra of 1,3-DMU[18], divided by a correction factor of 3.4 to account for differences in dynamics probed by the two methods,[14,19] yielding $\tau_{slow} = 7.35$ ps. Using this estimate, we describe the experimental data accordingly using eq. S5:

$$R(T_w) = R_0\{f_b e^{-T_w/\tau_{bulk}} + f_s e^{-T_w/\tau_{slow}}\} \qquad (S5)$$

Eq. S5 describes the experimental data equally well. The thus determined values of the fraction of water molecules with perturbed dynamics and the corresponding apparent hydration numbers are shown in Figure S3 together with the results of the analysis using eq. S4. As one would expect, imposing a faster time scale for the 'slow' water mode (~7 ps in eq. S5 *vs.* tens of ps in eq. S4) naturally translates into higher hydration numbers and slow water fractions. However, the markedly higher fraction of slowed-down water molecules due to 1,3-DMU, as compared to 1,1-DMU and 1-EU, is confirmed by this analysis.

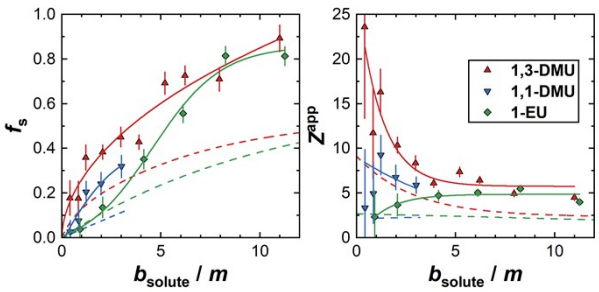

Figure S3. Slow water fraction, f_s, and the apparent hydration numbers, Z^{app}, obtained from the analysis of the anisotropy dynamics using a biexponential model (eq. S5 symbols and solid

lines). Dashed lines show the trend lines corresponding to an 'exponential + offset' model (eq. S4) for comparison.

CLS analysis at high solute concentration

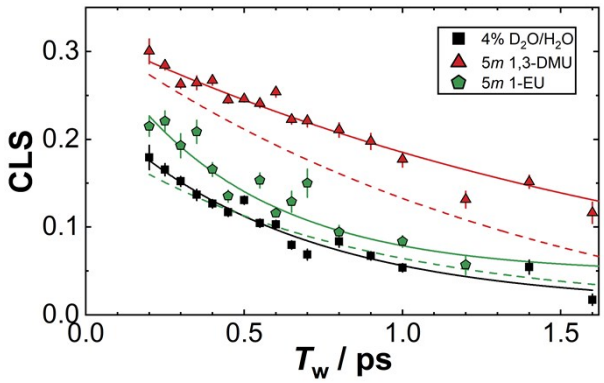

Figure S4. CLS dynamics of the bleach of v(OD) of trace HDO in 4% D_2O/H_2O as well as in 5 m solutions of 1-EU and 1,3-DMU. Solid lines are mere guides to the eye, while the dashed ones are trend lines for 3 m datasets from Figure 3B of the main text for comparison.

Estimation of the solvent accessible surface area of RUs

In order to assess the significance of congestion of the substituents on the excluded volume effect we computed the solvent accessible surface area (SASA) of the molecules of the studied RUs. To this end, atomic coordinates were obtained from geometry optimizations at the MP2/aug-cc-pvtz level of theory using implicit water environment within polarizable continuum model (PCM)[20] as implemented in GAUSSIAN 09.[21] SASA values were computed with VMD v. 1.93[22] assuming 1.6 Å probe size. The results are compiled in Table S1.

Table S1. Solvent accessible surface area (SASA, Å^2) of the studied RU molecules estimated using a probe radius of 1.6 Å

SASA	1,3-DMU	1,1-DMU	1-EU

Total	255	245	245
Alkyl	156	133	115
CO	49	55	48
NH_x	50	57	82

ESI References

1 H.-S. Tan, I. R. Piletic and M. D. Fayer, *J. Opt. Soc. Am. B*, 2005, **22**, 2009.

2 A. M. Dokter, S. Woutersen and H. J. Bakker, *Proc. Natl. Acad. Sci.*, 2006, **103**, 15355–15358.

3 S.-H. Shim and M. T. Zanni, *Phys. Chem. Chem. Phys.*, 2009, **11**, 748–761.

4 P. Hamm and M. T. Zanni, *Concepts and Methods of 2D Infrared Spectroscopy*, Cambridge University Press, Cambridge, 2011.

5 S.-H. Shim, D. B. Strasfeld, Y. L. Ling and M. T. Zanni, *Proc. Natl. Acad. Sci.*, 2007, **104**, 14197–14202.

6 C. Rauscher and R. Laenen, *J. Appl. Phys.*, 1997, **81**, 2818–2821.

7 C. T. Middleton, A. M. Woys, S. S. Mukherjee and M. T. Zanni, *Methods*, 2010, **52**, 12–22.

8 Y. L. A. Rezus and H. J. Bakker, *J. Phys. Chem. B*, 2009, **113**, 4038–4044.

9 Y. L. A. Rezus and H. J. Bakker, *J. Chem. Phys.*, 2005, **123**, 114502.

10 T. Steinel, J. B. Asbury, J. Zheng and M. D. Fayer, *J. Phys. Chem. A*, 2004, **108**, 10957–10964.

11 Y. L. A. Rezus and H. J. Bakker, *Proc. Natl. Acad. Sci.*, 2006, **103**, 18417–18420.

12 Y. L. A. Rezus and H. J. Bakker, *J. Phys. Chem. A*, 2008, **112**, 2355–2361.

13 Y. L. A. Rezus and H. J. Bakker, *Phys. Rev. Lett.*, 2007, **99**, 148301.

14 K.-J. Tielrooij, J. Hunger, R. Buchner, M. Bonn and H. J. Bakker, *J. Am. Chem. Soc.*, 2010, **132**, 15671–15678.

15 P. K. Verma, H. Lee, J.-Y. Park, J.-H. Lim, M. Maj, J.-H. Choi, K.-W. Kwak and M. Cho, *J.*

Phys. Chem. Lett., 2015, **6**, 2773–2779.

16 L. Piatkowski, K. B. Eisenthal and H. J. Bakker, *Phys. Chem. Chem. Phys.*, 2009, **11**, 9033.

17 G. Stirnemann, F. Sterpone and D. Laage, *J. Phys. Chem. B*, 2011, **115**, 3254–3262.

18 V. Agieienko, D. Horinek and R. Buchner, *Phys. Chem. Chem. Phys.*, 2017, **19**, 219–230.

19 J. Hunger, K.-J. Tielrooij, R. Buchner, M. Bonn and H. J. Bakker, *J. Phys. Chem. B*, 2012, **116**, 4783–4795.

20 G. Scalmani and M. J. Frisch, *J. Chem. Phys.*, 2010, **132**, 114110.

21 M. J. Frisch, G. W. Trucks, H. B. Schlegel, G. E. Scuseria, M. A. Robb, J. R. Cheeseman, G. Scalmani, V. Barone, B. Mennucci, G. A. Petersson, H. Nakatsuji, M. Caricato, X. Li, H. P. Hratchian, A. F. Izmaylov, J. Bloino, G. Zheng, J. L. Sonnenberg, M. Hada, M. Ehara, K. Toyota, R. Fukuda, J. Hasegawa, M. Ishida, T. Nakajima, Y. Honda, O. Kitao, H. Nakai, T. Vreven, J. A. Montgomery, J. E. Peralta, F. Ogliaro, M. Bearpark, J. J. Heyd, E. Brothers, K. N. Kudin, V. N. Staroverov, R. Kobayashi, J. Normand, K. Raghavachari, A. Rendell, J. C. Burant, S. S. Iyengar, J. Tomasi, M. Cossi, N. Rega, J. M. Millam, M. Klene, J. E. Knox, J. B. Cross, V. Bakken, C. Adamo, J. Jaramillo, R. Gomperts, R. E. Stratmann, O. Yazyev, A. J. Austin, R. Cammi, C. Pomelli, J. W. Ochterski, R. L. Martin, K. Morokuma, V. G. Zakrzewski, G. A. Voth, P. Salvador, J. J. Dannenberg, S. Dapprich, A. D. Daniels, Farkas, J. B. Foresman, J. V Ortiz, J. Cioslowski and D. J. Fox, *Gaussian 09, Revis. B.01, Gaussian, Inc., Wallingford CT*, 2009.

22 W. Humphrey, A. Dalke and K. Schulten, *J. Mol. Graph.*, 1996, **14**, 33–38.